Unlocking New In-Situ Defect Detection Capabilities in Additive Manufacturing with Machine Learning and a Recoater-Based Imaging Architecture

Matteo Bugatti, Marco Grasso, and Bianca Maria Colosimo

Abstract Additive manufacturing (AM) has the potential to revolutionize the way products are designed and produced in a wide range of industries. However, ensuring the quality and reliability of AM parts remains a challenge, as defects can occur during the building process. In-situ monitoring is a promising approach for detecting and classifying these defects for in-process part qualification. In this paper, we present a novel approach for in-situ monitoring of laser powder bed fusion (LPBF) processes using a recoater-based imaging sensor and machine learning algorithms. The new sensor architecture is a recoater-mounted contact image sensor (CIS) and allows for high-resolution imaging of the build area during the recoating process, enabling the observation of a wide range of part and process-related defects. We demonstrate the effectiveness of using machine learning for image analysis on a series of experiments on a commercial AM system, showing significant improvements in defect detection accuracy compared to existing methods. Our results demonstrate the potential of the recoater-based sensor architecture for unlocking new capabilities for in-situ monitoring and quality control in powder bed-based AM processes.

Keywords Additive manufacturing · In-situ monitoring · Recoater-based imaging sensor

1 Introduction

Quality assurance of AM products is crucial to ensure functionality and safety of the products. Metal AM can suffer from a wide range of defects such as porosity, cracks, and inclusions. These defects are often generated during the AM process itself and it can be challenging to detect them in the final product. This is especially true when dealing with complex structures that are more difficult to inspect with

M. Bugatti (✉) · M. Grasso · B. M. Colosimo
Dipartimento Di Meccanica, Politecnico Di Milano, Via La Masa 1, 20156 Milano, MI, Italy
e-mail: matteo.bugatti@polimi.it

traditional non-destructive testing (NDT) methods [1]. Over the past several years, there has been a growing interest in in-situ monitoring of AM processes to detect and classify defects in real-time. This approach leverages the "openness" of the AM process, which allows for the observation of the build area during the process, and it is considered to have the potential to significantly reduce the cost of quality control and, in the future, improve the overall quality of AM parts via a combination of in-situ monitoring and process control.

A wide variety of monitoring techniques have been explored in the literature, both image (e.g. optical, thermal and x-ray imaging) and non-image based methods (e.g. acoustic emission and ultrasonic) [2]. However, most of these methods suffer from one or more of the following limitations: (i) low spatial resolution, (ii) small field of view or (iii) limited applicability to industrial AM processes. Optical imaging methods are among the most popular in-situ monitoring techniques for AM processes. Newer industrial machines are usually equipped with one external camera pointed at the build platform. The camera is used to take images of the printed area and of the surrounding powder bed throughout the build process. These images can be used to detect some powder bed inhomogeneities, such as incomplete spreading, powder streaking or recoater hopping. However, these methods are limited to detecting large-scale defects and are not suitable for smaller powder bed defects, such as contaminations. In addition, the low resolution does not allow to perform part reconstruction or detect small-scale defects that may appear on the top surface of the printed part (e.g., open pores, balling etc.).

To unlock the full potential of optical imaging for AM in-situ monitoring, it is necessary to combine high-resolution imaging with a field of view that is large enough to cover the entire build area. In a recent work [3], we demonstrated the implementation of a recoater-mounted contact image sensor (CIS) for in-situ monitoring of LPBF processes. The type of sensor, which is often used in other quality control applications, and its position in the build chamber offer several advantages over the traditional external camera. In addition to the large field of view and higher resolution, the CIS offers the ability to capture color images and, thanks to the integrated lighting system, provides a more homogeneous illumination across the scene. These two additional features contribute to significantly improve the image quality compared to external cameras. Other authors [4], using a similar architecture, have also demonstrated that by leveraging an additional feature of the sensor, i.e., the extremely short focal length, a pseudo height map can be reconstructed from the images. This allows to detect out-of-plane defects in the powder bed and on the printed parts, but the accuracy is limited and the "direction" of the deviation (e.g., whether the out-of-plane is a peak or a valley) cannot be determined.

In this paper, we explore the impact of this new sensor architecture on the performance of a machine learning algorithm for detecting dimensional and geometrical deviations in the printed part. A comparative study between the recoater-mounted CIS and the external camera is also presented to highlight differences and potential limitations of the two architectures.

2 Equipment and Experimental Setup

The case study investigated in this paper is a test print of a series of bridge samples printed with different support structures. The test print was performed on a commercial LPBF system (3D-NT) equipped with a recoater-mounted CIS and an external camera module. The specifications of the two sensors are summarized in Table 1.

The four samples were printed using the same process parameters reported in Table 2.

The only difference between the samples is the support strategy used. The bridge-like geometry was specifically designed to enhance the stress-induced deformation. Table 3 summarizes the main characteristics of the four support structures shown in Fig. 1.

The standard support strategy (Fig. 1a) serves as a baseline to compare against the other, increasingly weaker, support structures.

Table 1 Monitoring equipment

	CIS	Camera
Working distance (WD) [mm]	14	500
Resolution [μm/px]	21	100
Mode	Color	Mono
Depth	8-bit	8-bit

Table 2 Process parameters

Parameter	Value
Power [W]	200
Scan speed [mm/s]	1000
Hatch distance [μm]	90
Scan strategy	Hatching
Layer thickness [μm]	25
Build plate material	AlSi10Mg
Focal position f [mm]	0
Beam waist diameter D4σ [mm]	0.05

Table 3 Types of support structures

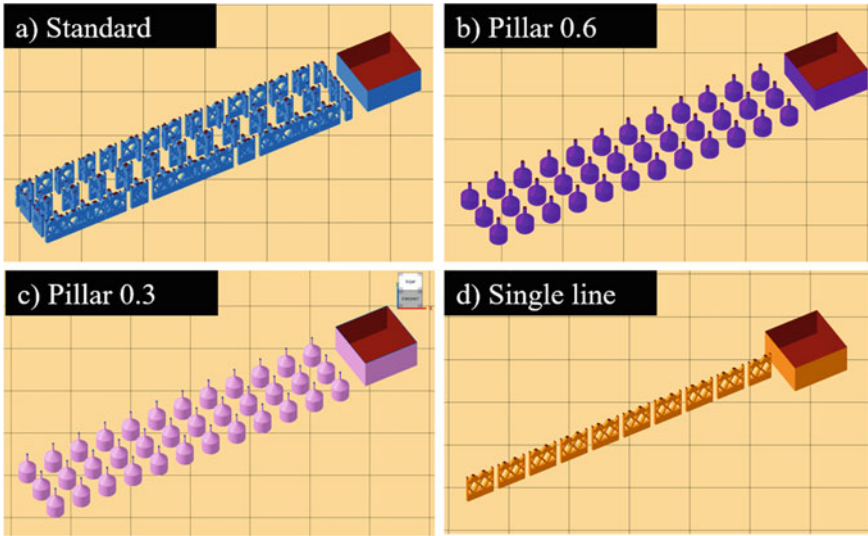|	Standard	Pillar 0.6	Pillar 0.3	Single line
Shape	Lattice wall	Pillar	Pillar	Lattice wall
Thickness/diameter [mm]	0.5	0.6	0.3	0.5
Distance btw. walls/pillars [mm]	5	5	5	–
Support-Part connection	Triangular	Rounded	Rounded	Triangular

Fig. 1 Types of support structures

This experiment investigates the well-known trade-off between buildability and post-processing costs. Robust support structures make it easier to print the part, but they add complexity to the post-processing operations (i.e., support removal).

On the other hand, weaker support structures simplify the post-processing and increase the cost-effectiveness of production, but they are more likely to fail under residual stress load. If some supports fail, the printed part will lack fixed anchor points, which can lead to geometrical and dimensional deviations from the original design. Excessive deviations result in a part that is out of tolerance and must be scrapped, thus increasing the cost of production, and reducing the overall efficiency of the process.

In this scenario, the application of in-situ monitoring can be beneficial and allow to monitor the integrity of support structures to prevent the onset of critical deviations and stop the build process to prevent the production of a defective part and minimize waste.

To validate the results of the in-situ monitoring method developed in this work, the geometrical and dimensional deviations of the samples were measured ex-situ via CT-scan.

3 Methodology

The integrity of support structures can be monitored either directly or indirectly. Direct monitoring of the support structures consists in observing the support structures during the build process. Due to the typical size of the support stuctures, direct monitoring is only possible with high-resolution sensors, such as the recoater-mounted CIS.

The indirect way of monitoring the support structures consists in observing the behavior of the supported part during the build process. When the support fails under residual stress load, the supported part will start warping. As soon as the warping exceeds the powder bed thickness (typically less than 0.1 mm), the recoater will fail to spread the powder over the warped portion of the part and the part will remain exposed. The incomplete powder spreading can be observed in the layerwise images, and it can be used to infer the integrity of the support structures, or the lack of support structures altogether.

In the literature, there are several examples of algorithms capable of detecting defects associated to powder bed inohomogenities. For example, Zhang et al. [5], report they can detect height differences in each printed layer, while Zur Jacobsmuhlen et al. [6, 7] in two different studies specifically worked on super-elevated edges, and developed a method to classify them into critical and non-critical classes. Scime et al. [8, 9] developed a classifier based on deep convolutional neural networks to identify recoating defects, such as streaking, hopping and super-elevation.

In this work, a new method was developed to automatically detect part warping and other phenomena that affect the powder spreading using the in-situ images. The main steps of the algorithm are briefly outlined in the following:

1. *Pre-processing*: perspective and flat field correction.
2. *Masking*: the regions of interest (RoI) corresponding to each printed part at layer i are isolated in the corresponding post-deposition image using the nominal slice of layer i as a reference.
3. *Empirical probability density function (PDF)*: the histogram of the region of interest was extracted.
4. *Dimensionality reduction*: the simplicial functional principal component analysis (SFPCA) is performed to find the directions along which the dataset displays the maximum variability. The first K principal components are retained based on the percentage of explained variability.
5. *Scores calculation*: the first K scores are then used to analyze the dataset.

In a preliminary step, flat field and perspective corrections (homography) are applied to the layerwise images obtained from the recoater-mounted CIS and the external camera to get a top-down view of the build area, similar to the nominal layerwise images. The images are then registered and cropped to match the size of the corresponding nominal slice and the position of the parts. After registration, the images are smoothed and the pixel intensity is modified to correct for broad illumination inhomogeneities.

Compared to the external camera images (Fig. 2), the unprocessed CIS images (Fig. 3) already provide a close to perfect top-down view of the build platform. Only minor corrections must be performed to adjust for alignment errors when mounting the CIS on the recoater. This results in a final image that is less distorted and higher quality.

After the preliminary steps and the image pre-processing is complete, the masking step is performed (Fig. 4). This operation makes the method completely shape-agnostic and exploits the nominal slice shape as prior knowledge about the area where to look for powder bed inhomogeneity anomalies. A "dilated" version of the
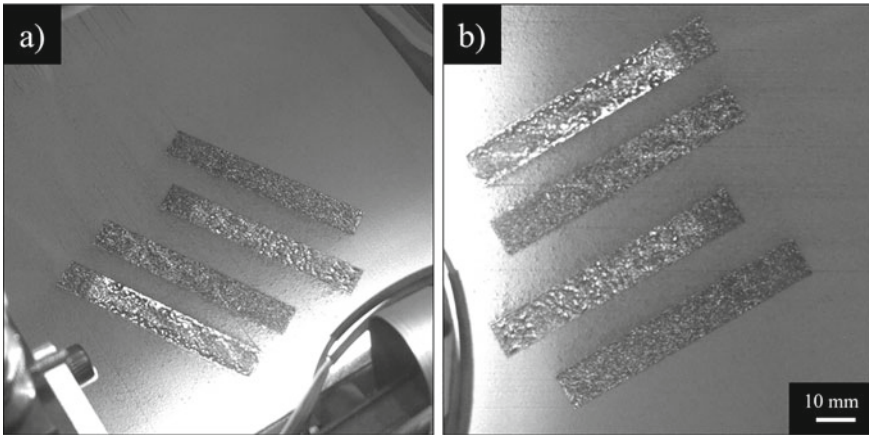
Fig. 2 Homography operation on external camera images, before (**a**) and after (**b**)
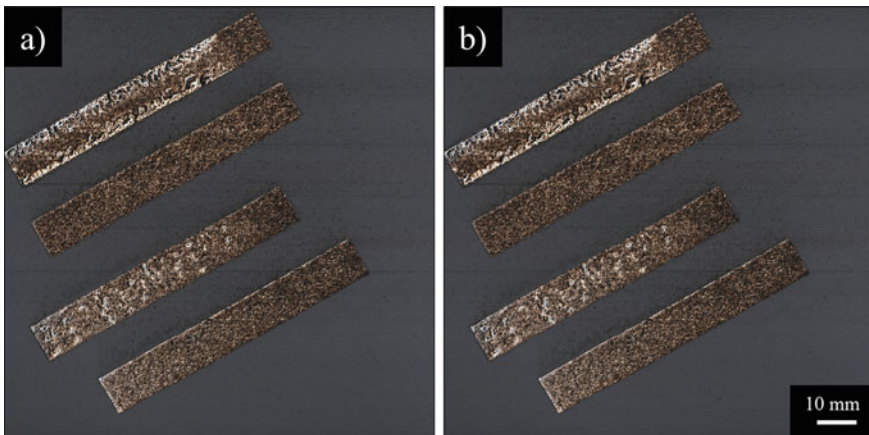

Fig. 3 Perspective correction on CIS images, before (**a**) and after (**b**). Almost no correction is required in this case
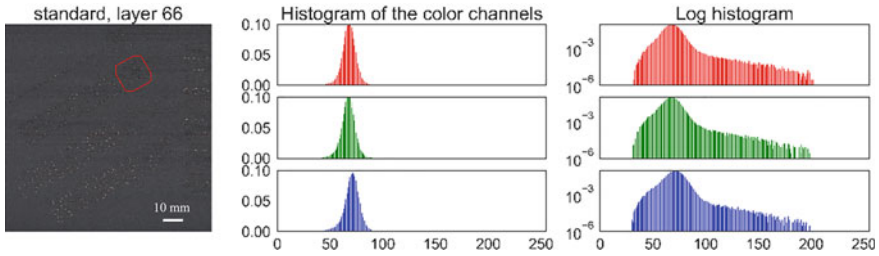
Fig. 4 Extraction of the empirical PDF function from the ROI

mask of each part is applied to make sure to include some of the surrounding powder for reference.

The extraction of the empirical PDF is then performed for each individual masked area (i.e., each individual part). The intuition behind this approach is that functional data that represent the empirical PDF will differ when the ROI under analysis contains only an homogeneous powder layer (i.e., in control condition) or powder and a portion of the part (i.e., out-of-control condition).

However, dealing with functional datasets can be complex due to the intrinsic high dimensionality (Fig. 4). For this reason, a dimensionality reduction step was implemented. Simplicial functional principal component analysis (SFPCA) [10] was used for this task. SFPCA is a specific counterpart of the traditional FPCA which is performed within the space of density functions (Bayes space B2), and allows to obtain a high-quality approximation of PDFs, while preserving their constraints. This method was originally developed by Menafoglio et al. [11] to monitor the quality of metal foams from the empirical PDF of specific variables of interest. In this work, the same approach SFPCA-based was used to reduce the dimensionality of the dataset.

The SFPCA procedure finds the directions in B^2 along which the variability of the dataset is maximized. Using the associated eigenvalues, ρ_i, computed from the SFPCA, it is possible to identify the minimum number, K, of SFPCs needed to retain a specific amount of the total variability, according to Eq. (1):

$$\sum_{i=1}^{K} \rho_i \bigg/ \sum_{i=1}^{\infty} \rho_i \tag{1}$$

The first K scores, i.e., the projection of the original empirical PDFs along the first K principal directions, were then used to study the problem in a low dimensional space with respect to that of the original functional dataset.

4 Discussion of Results

Two main types of defects were found during the print, i.e., the presence of warping (Fig. 5) or incomplete recoating of the part (Fig. 6).
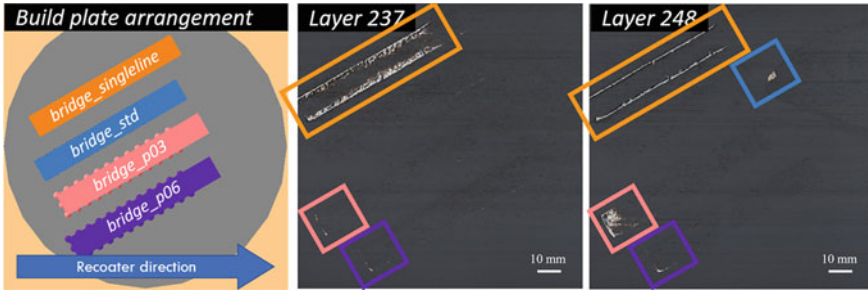
Fig. 5 Post-deposition images showing different stages of the warping defect in the sample with single line support
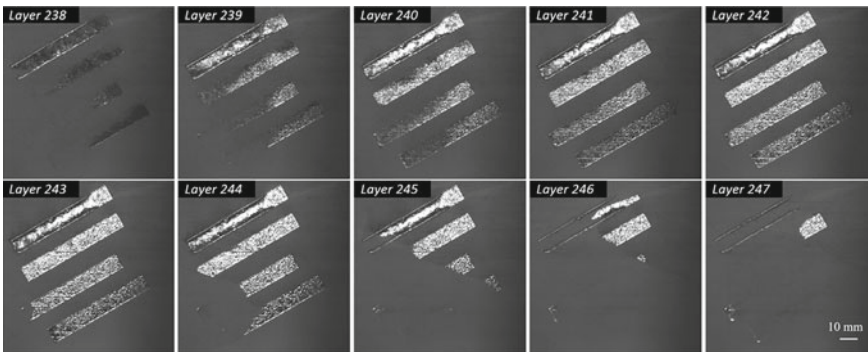

Fig. 6 Incomplete spreading due to insufficient powder feed (layer 238–247)

The detected anomalies match very closely the defects observed in the CT-scan (Figs. 7 and 8).

The samples printed with the standard and the pillar 0.6 mm support structures (Fig. 7a, b) showed no significant deviations from the nominal shape. All the supports were intact at the end of the print, which confirms that the support structures were robust enough to withstand the residual stress load.

Significant warping was observed immediately after printing the first overhang layers of the least supported sample, i.e., the bridge with single line supports. The lack of anchor points on the sides of the sample resulted in a visible deformation and consequent deviation from the nominal shape.

The bridge with 0.3 mm pillar supports showed an intermediate behavior. The supports were able to withstand the residual stress load for the first few layers, after which the supports subjected to the highest load (i.e., near the edge) started to fail. The final deformation of the bridge exceeds 2 mm near its most extreme region.

The incomplete spreading, on the other hand, led to a thicker layer of powder being deposited when powder supply was restored. Since the energy density was not sufficient to fully melt such a thick layer of powder, gaps and delaminations are
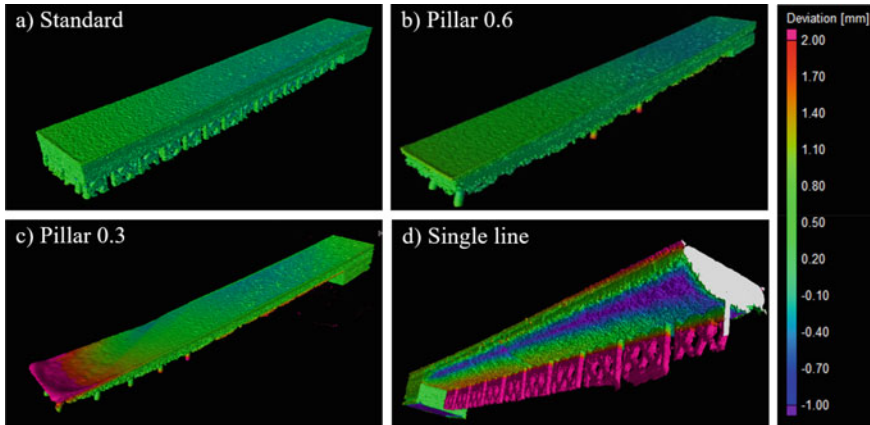
Fig. 7 CT-scan of the bridge samples. The most supported samples, i.e., standard (**a**) and pillar 0.6 (**b**), show little to no deformation, unlike the least supported ones, i.e., pillar 0.3 (**c**) and single line (**d**)
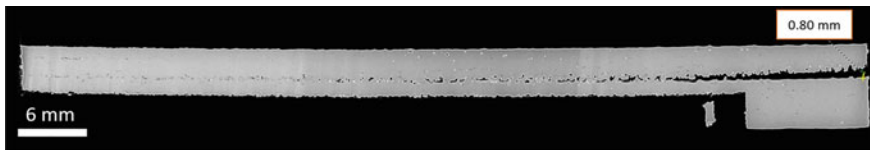

Fig. 8 Lack-of-fusion and delamination in the standard supports sample due to incomplete spreading from layer 238 to 247

observed at that specific layer height due to lack-of-fusion and incomplete bonding between the new layer and the existing part (Fig. 8).

When large deviations occur, i.e., an extended region of the part is not covered by the new powder layer, the empirical PDFs show a significant departure from the standard unimodal distribution that is expected in the histogram of a well recoated region. The empirical PDFs extracted from two different groups of images, in-control (from layer 50–70) and out-of-control (from layer 230–250) are show in Fig. 9.

After applying the SFPCA procedure and computing the eigenvalues and eigen-functions, it is possible to see that the only first 2 SFPCs are necessary to retain almost 90% of the total variability (Fig. 10).

The scores for the two sets of observations (in-control and out-of-control) are shown in Fig. 11. Two well separated clusters are clearly visible in the scatterplot. This means that, just by using the first 2 scores of the SFPCA, in-control and out-of-control PDFs can be immediately identified.

The same approach was tested on the external camera images, but the results were not on par with the CIS (Fig. 12). The separation between in-control and out-of-control clusters is not as clear and some out-of-control observations fall close to the in-control ones.
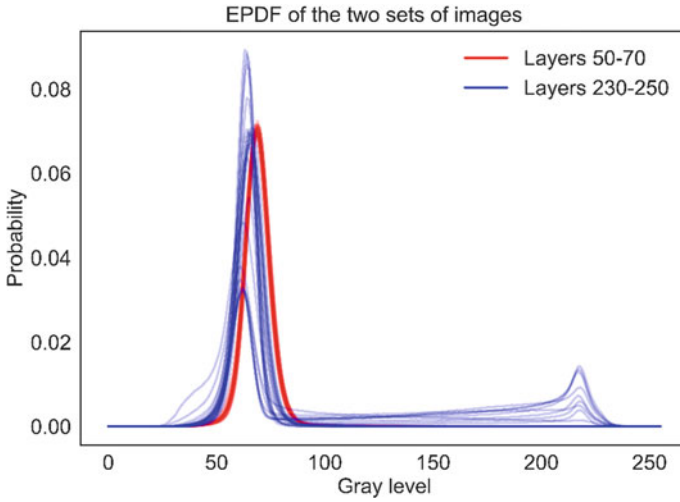
Fig. 9 Comparison between the in-control (layer 50–70) and out-of-control (layer 230–250) empirical PDFs (CIS images) of the standard supports sample
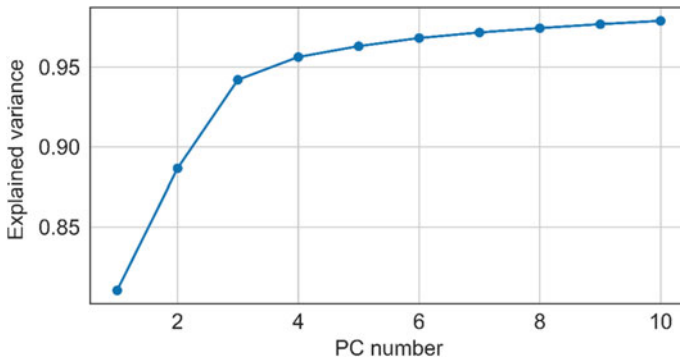

Fig. 10 Explained variance of each PC

Despite the layers under analysis being the exact same, the difference in perfor-mance is most probably related to the lower quality images acquired by the external camera. The empirical PDFs extracted from the camera images (Fig. 13) show a noisier distribution, even when considering only the in-control conditions. This is likely the root cause of the lower precision of the external camera at detecting shifts in the distribution using principal components scores.

A direct comparison between the images of the two sensors is shown in Fig. 14. The CIS allows to inspect the part at an unprecedented resolution, giving the ability to observe surface patterns that are not visible to the external camera. The images of the recoater-mounted CIS provide a better contrast between the powder and the
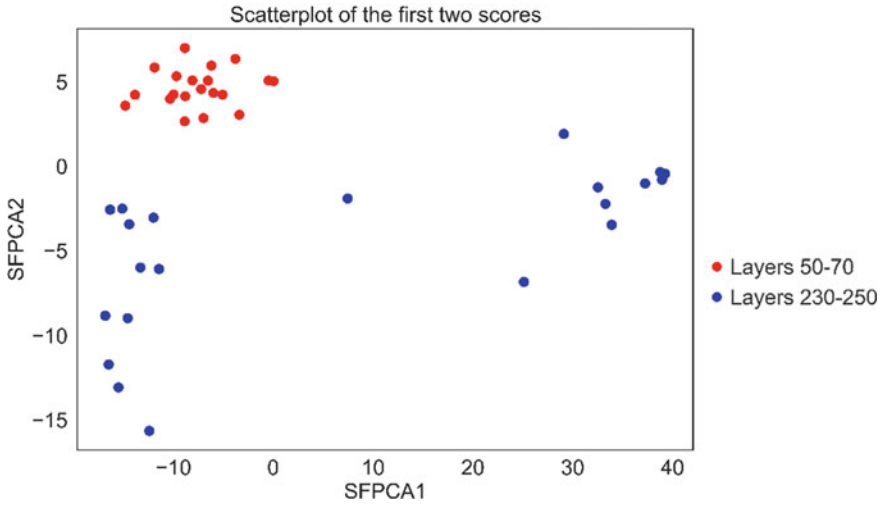
Fig. 11 First 2 scores of the in-control and out-of-control empirical PDFs extracted from the CIS images
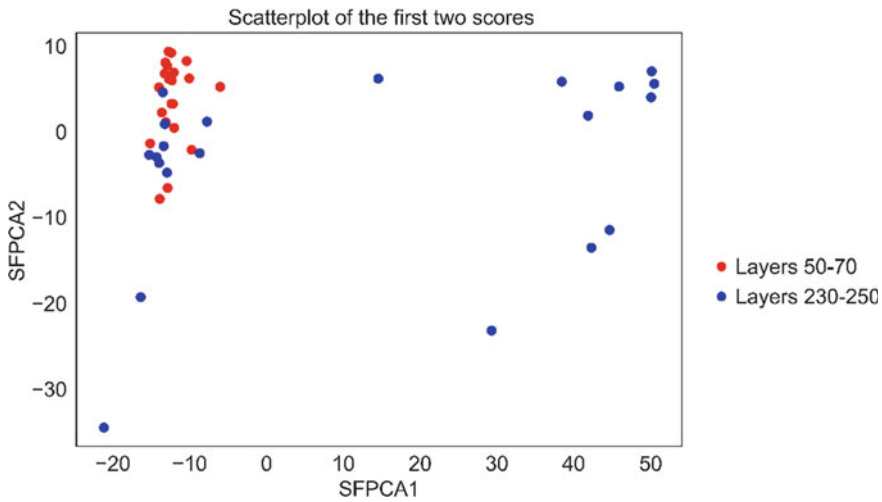

Fig. 12 First 2 scores of the in-control and out-of-control empirical PDFs extracted from the external camera images

printed part, and three distinct types of surface patterns can be observed, depending on the phase of the powder, i.e., (i) fully melted powder, (ii) partially melted powder, and (iii) unmelted powder. On the other hand, the images of the external camera show a more uniform surface, with no visible differences between some surface pattern (e.g., unmelted and partially melted powder).
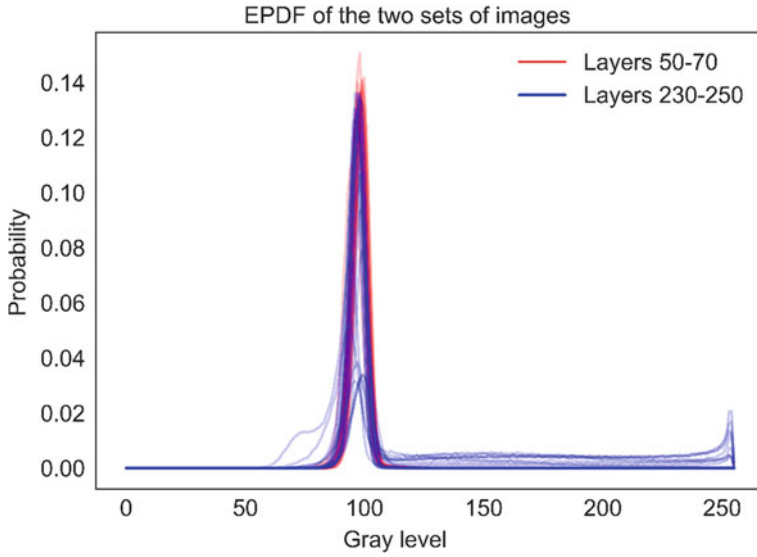
Fig. 13 Comparison between the in-control (layer 50–70) and out-of-control (layer 230–250) empirical PDFs (external camera images) of the standard supports sample
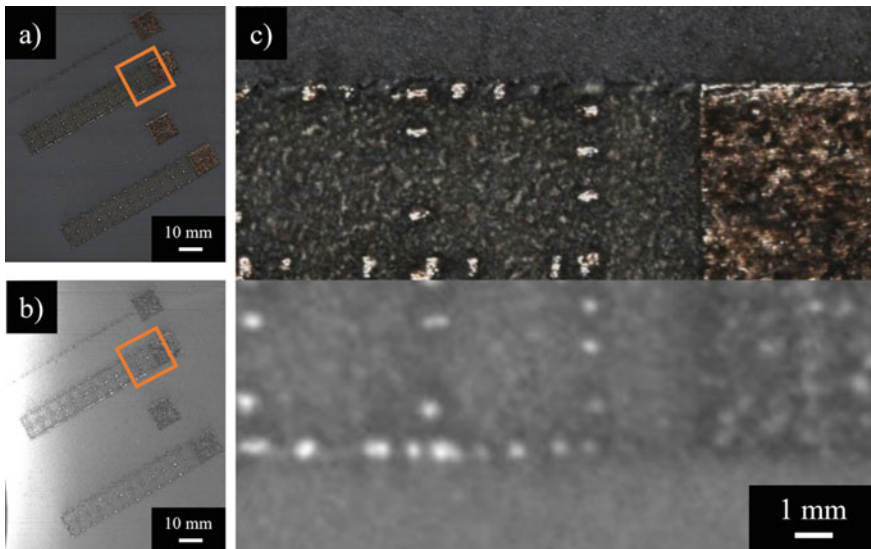

Fig. 14 Image quality comparison. Full images from the CIS (**a**) and the external camera (**b**) and side by side comparison (**c**) (CIS on the top, and camera on the bottom)

5 Conclusion and Future Work

In this paper, we have presented a comparative study between the recoater-mounted CIS and the external camera for in-situ monitoring of LPBF processes. The results of this study show that the recoater-mounted CIS is a promising sensor architecture for in-situ monitoring of LPBF processes and it can be used to detect the onset of critical deviations in the printed part. Compared to the external camera, the recoater-mounted CIS is more precise at detecting critical deviations in the image composition that are not as clear to the external camera. This translates to a quicker detection of deviations before they exceed the tolerance limits, and the part needs to be scrapped. This higher precision can be used to act earlier on the process and, when possible, adjust the printing strategy to recover from the deviation and save the part rather than stopping its production altogether.

This study primarily concentrated on identifying large-scale deviations in the components. However, the high-resolution images obtained by the recoater-mounted CIS can be utilized to detect small-scale defects by implementing the empirical PDF-based technique on smaller areas of the powder bed. Future research will focus on detecting other types of defects, such as spatters and contamination, which are not visible to conventional inspection methods but are known to cause the development of porosity and inclusions in the finished product.

References

1. Colosimo BM, Huang Q, Dasgupta T, Tsung F (2018) Opportunities and challenges of quality engineering for additive manufacturing. J Qual Technol 50(3):233–252
2. Grasso M, Remani A, Dickins A, Colosimo BM, Leach RK (2021) In-situ measurement and monitoring methods for metal powder bed fusion: an updated review. Meas Sci Technol 32(11):112001
3. Bugatti M, Colosimo BM (2022) The intelligent recoater: a new solution for in-situ monitoring of geometric and surface defects in powder bed fusion. Addit Manuf Lett 3:100048
4. Seita M (2019) A high-resolution and large field-of-view scanner for in-line characterization of powder bed defects during additive manufacturing. Mater Des 164:107562
5. Zhang B, Ziegert J, Farahi F, Davies A (2016) In situ surface topography of laser powder bed fusion using fringe projection. Addit Manuf 12:100–107. https://doi.org/10.1016/j.addma.2016.08.001
6. Zur Jacobsmuhlen J, Kleszczynski S, Schneider D, Witt G (2013) High resolution imaging for inspection of Laser Beam melting systems. In: 2013 IEEE international instrumentation and measurement technology conference, pp 707–712. https://doi.org/10.1109/I2MTC.2013.6555507.
7. Zur Jacobsmuhlen J, Kleszczynski S, Witt G, Merhof D (2015) Detection of elevated regions in surface images from laser beam melting processes. In: IECON 2015-41st annual conference of the ieee industrial electronics society, pp 1270–1275. https://doi.org/10.1109/IECON.2015.7392275
8. Scime L, Beuth J (2018) A multi-scale convolutional neural network for autonomous anomaly detection and classification in a laser powder bed fusion additive manufacturing process. Addit Manuf 24:273–286

9. Scime L, Siddel D, Baird S, Paquit V (2020) Layer-wise anomaly detection and classification for powder bed additive manufacturing processes: a machine-agnostic algorithm for real-time pixel-wise semantic segmentation. Addit Manuf 36:101453

10. Hron K, Menafoglio A, Templ M, Hrůzová K, Filzmoser P (2016) Simplicial principal component analysis for density functions in Bayes spaces. Comput Stat Data Anal 94:330–350

11. Menafoglio A, Grasso M, Secchi P, Colosimo BM (2018) Profile monitoring of probability density functions via simplicial functional PCA with application to image data. Technometrics 60(4):497–510